Coastal Engineering 73 (2013) 178–190

Contents lists available at SciVerse ScienceDirect

Coastal Engineering

journal homepage: www.elsevier.com/locate/coastaleng

Numerical modeling of low-frequency wave dynamics over a fringing coral reef

Ap Van Dongeren [a,*], Ryan Lowe [b], Andrew Pomeroy [a,b,d], Duong Minh Trang [a,c], Dano Roelvink [a,c], Graham Symonds [e], Roshanka Ranasinghe [c,d]

[a] Deltares, P.O Box 177, 2600 MH, Delft, The Netherlands
[b] The University of Western Australia, School of Earth and Environment and UWA Oceans Institute, 35 Stirling Highway, Crawley, WA, 6009, Australia
[c] UNESCO-IHE, P.O. Box 3015, 2601 DA, Delft, The Netherlands
[d] Delft University of Technology, Faculty of Civil Engineering and Geosciences, Section Hydraulic Engineering, P.O. Box 5048, 2600 GA, Delft, The Netherlands
[e] CSIRO Marine and Atmospheric Research, Private Bag 5, Wembley, WA, 6913, Australia

ARTICLE INFO

Article history:
Received 21 August 2012
Received in revised form 9 November 2012
Accepted 20 November 2012
Available online 21 December 2012

Keywords:
Fringing reef
Infragravity waves
Wave transformation
Currents
Waves
Hydrodynamics

ABSTRACT

Low-frequency (infragravity) wave dynamics on a fringing coral reef were investigated using the numerical model XBeach (Roelvink et al., 2009). First, the skill of the model was evaluated in one- and two-dimensions based on its predictions of short waves (0.04–0.2 Hz), infragravity waves (0.004–0.04 Hz) and water level measurements (tidal and wave setup) obtained during a 2009 field study at Ningaloo Reef in Western Australia. The model calibration was sensitive to friction coefficients for short waves and current/infragravity bed friction, which were assumed independent in this model study. Although the one-dimensional cross-shore model captured the gradients in the dominant hydrodynamic processes at the site, a high current/IG bed friction coefficient was required. This resulted in an overestimation and a phase lag between the observed and predicted wave setup signal. In the two-dimensional model, a lower (more realistic) current/infragravity wave friction coefficient was required to achieve optimum performance due to the presence of significant reef and lagoon mean flows in the model, which led to reduced setup across the reef. The infragravity waves were found to propagate from the surf zone across the reef in a dominantly cross-shore direction towards the shore, but with substantial frictional damping. The infragravity waves were strongly modulated also over the reef by tidal depth variations, primarily due to the variability in frictional dissipation rates when the total water depth over the reef varied. Two mean wave-driven circulation cells were observed in the study area, with cross-shore flow becoming more alongshore-dominated before exiting the system via the two channels in the reef. The results reveal that short waves dominated bottom stresses on the forereef and near the reef crest; however, inside the lagoon, infragravity waves become increasingly dominant, accounting up to 50% of the combined bottom stresses.

1. Introduction

A large proportion of the world's coastlines, perhaps as high as 80% (Emery and Kuhn, 1982), contain a broad class of submerged reef structures, including tropical coral reefs, relic temperate limestone platforms and rocky coastal features. Abundant as these structures may be, comparatively little work (as compared to sandy beaches) has addressed the range of nearshore hydrodynamic processes in reef environments. A good understanding of these processes is important because waves and wave-induced currents on reefs ultimately drive sediment transport (e.g., Storlazzi et al., 2004), nutrient dynamics and uptake by benthic reef communities (e.g., Falter et al., 2004), as well as the transport and dispersal of larval fish and other organisms (e.g., Wolanski and Sarsenski, 1997) in these environments. Hydrodynamics are thus important for the morphological development of reef environments and their associated ecological zonation (e.g., Atkinson and Falter, 2003; Kench and Brander, 2006). While reefs protect the coast by dissipating wave energy offshore, severe coastal erosion and flooding may still take place during typhoons and hurricanes (e.g., Ogg and Koslow, 1978; Péquignet et al., 2009). Thus, the impact of environmental changes on a reef and the adjacent coastline (e.g. climate-induced sea level rise), extreme events and/or human interventions can only be accurately predicted with sufficient knowledge of nearshore processes.

Of the three main types of tropical coral reefs (barrier, atoll and fringing reefs), fringing reefs form adjacent to a mainland coast, and will therefore have the most direct interaction with it. Darwin (1842) first hypothesized that reef-building corals grow best in regions of a reef experiencing moderate wave energy, i.e., "It appears, […] that the action of the surf is favorable to the vigorous growth of the stronger corals, and that sand or sediment, if agitated by the waves, is injurious to them." Darwin was also the first to refer to wave-induced mass flux and subsequent circulation: "a return stream

* Corresponding author. Tel.: +31 15 285 8951; fax: +31 15 285 8712.
E-mail address: Ap.vanDongeren@Deltares.nl (A. Van Dongeren).

0378-3839/$ – see front matter © 2012 Elsevier B.V. All rights reserved.
http://dx.doi.org/10.1016/j.coastaleng.2012.11.004

must carry away the water thrown over the outer edge; and the current thus produced, would tend to prevent the channel being filled up with sediment." However, the detailed mechanisms controlling hydrodynamic variability over reefs were not elucidated at that time.

Munk and Sargent (1948) first quantified a mean wave set up of several decimeters relative to mean sea level over the reef at Bikini Atoll. This set up can be explained using radiation stress theory (Longuet-Higgins and Stewart, 1964) in which the decrease in wave energy flux due to wave breaking is (partially) balanced by a gradient in the mean water set up over the reef. Lee and Black (1978) and Hardy and Young (1996) observed the considerable transformation of incident short waves dominated by swell, in terms of wave heights and the spectral redistribution from higher to lower frequencies as the waves broke over the reef. Other field studies have specifically investigated how the transformation of short waves (e.g., swell) on reefs generates mean wave-driven currents across reef systems, primarily due to wave breaking (e.g., Hench et al., 2008; Jago et al., 2007; Lowe et al., 2009a; Symonds and Black, 2001; Taebi et al., 2011). Symonds et al. (1995) first formulated an analytical model based on a linearized set of momentum equations in order to demonstrate the relative importance of set-up and onshore wave-driven flow across an idealized 1D reef system (subsequent 1D analytical models were also formulated by Hearn (1999) and Gourlay and Colleter (2005)).

Despite physical differences between sandy coast and reef environments, simple 1D (cross-shore) wave transformation models developed for mildly-sloping beaches have been successfully used to investigate short wave transformation over some reefs. Gerritsen (1980) and Lowe et al. (2005) used a 1D wave-energy conservation model with the Battjes and Janssen (1978) breaker model, and both Massel and Gourlay (2000) and Sheremet et al. (2011) extended a mild-slope equation model with a correction for the steeper slopes of reefs.

More complex two-dimensional horizontal (2DH) and three-dimensional (3D) coupled wave-circulation numerical models have also been developed to predict the spatial distribution of mean wave-driven currents and water levels within reef-lagoon systems (Lowe et al., 2009b; Ranasinghe et al., 2006; Symonds and Black, 2001). These models are in essence based on the equation of mass conservation and the equations of 2D or 3D horizontal momentum conservation driven by radiation stress gradients, which are computed from the 2D quasi-steady conservation of short wave energy equation with dissipation terms for wave breaking and bottom friction dissipation.

Collectively, these field and modeling reef studies have shown that the physical processes on reefs do have some similarities to those on sandy coasts (e.g., having submerged bars), albeit with some important differences: the slope of reefs is generally much steeper than the foreslope of sandy shores, the reef bottom topography is much rougher and more inhomogeneous, and there is typically a larger distance between the breakpoint of the waves and the coastline.

Despite the historical focus on the dynamics of short wave energy (periods of 5–25 s) and mean (i.e. averaged over many wave periods) wave-driven flows on reefs, a relatively small number of field studies have identified the importance of lower frequency wave motions (periods of 25 s to tens of minutes), termed infragravity (IG) waves, to the overall water motion over coral reef flats and lagoons (e.g., Brander et al., 2004; Hardy and Young, 1996; Lugo-Fernandez et al., 1998). In particular, two recent field studies (Péquignet et al., 2009 and Pomeroy et al., 2012) have shown that mean currents and short waves accounted for only a small part of the total observed flow and surface elevation variance in the region between the reef crest and the shoreline of two fringing reefs with very different morphologies. Instead, the bulk of the water level variability was found to be contained within the IG frequency band, despite the response of the IG waves being somewhat different between systems. Péquignet et al. (2009) observed a cross-reef standing waves over a fringing reef flat in Guam while Pomeroy et al. (2012) observed dominantly shoreward propagating IG waves across the lagoon over a fringing reef in Western Australia.

Despite the importance of IG wave motions to reefs, process-based numerical models capable of predicting their dynamics have been lacking. Recently Nwogu and Demirbilek (2010) and Sheremet et al. (2011) each applied a 1D phase-resolving wave model to simulate both short wave and IG waves from laboratory flume experiments. They found that the models were capable of predicting the overall wave transformation and spectral redistribution (including IG waves) fairly well. However, these experiments used a scaled fringing reef prototype with smooth walls (no bottom roughness). Consequently, bottom friction in these models was either minimal (Nwogu and Demirbilek, 2010) or neglected entirely (Sheremet et al., 2011), so that IG wave decay was dominated by nonlinear momentum transfers (Henderson et al., 2006; Sheremet et al., 2011). 2DH or 3D numerical modeling studies of IG wave dynamics over real reefs (incorporating their full topographic complexity and importantly their large bottom friction coefficients) have yet to be conducted. Roeber and Cheung (2012) described an application of a 2D Boussinesq-type model to fringing reefs. They showed good model comparison to laboratory data of solitary wave incident on a 1D and 2D reef. The model was applied to a field site in Hawaii, showing for two steady-state conditions, the transformation of irregular incident waves, wave-induced setup and development of sub (infragravity band) and super-harmonics, but without conducting a detailed investigation into the dynamics. The objective of this paper was to investigate and understand the dynamics of IG wave motions across a fringing coral reef. This was done through an application of a recently-developed nearshore circulation model (XBeach) (Roelvink et al., 2009) that includes IG wave generation, propagation and decay, to a case study of Ningaloo Reef, a large fringing reef located on the northwest coast of Western Australia. In particular, attention is given to determining (a) the processes governing IG wave generation and decay over the reef, and (b) the relative importance of IG waves, short waves and currents on the spatial distribution of bed shear stresses, induced by water motion in the lee of the reef crest.

The paper is organized as follows. The field experiment is briefly described in Section 2. The XBeach model and the input parameters adopted for this study are discussed in Section 3. The results of the one- and two-dimensional model calibrations are then presented in Section 4. In Section 5, the validated 2DH model is used to investigate the dynamics of the IG waves under scenarios of different mean water levels, including their generation and dissipation, their propagation and finally the relative importance of IG waves, short waves and currents on bed shear stresses throughout the reef-lagoon system. The factors that affect the performance of the model are discussed in Section 6 along with the dynamics of IG waves that have been elucidated in this study. We finish with conclusions in Section 7.

2. Field study

This study focuses on the hydrodynamics occurring within an ~7 km section of Ningaloo Reef at Sandy Bay (Fig. 1a and b), which is composed of a shallow reef flat (~1–2 m depth) that is separated from the shore by a slightly deeper lagoon (~2–3 m average depth). The reef is broken to the north and south of the study area by channels, through which water exchange between the lagoon and the ocean occurs (Taebi et al., 2011). This present study employs data from a field experiment conducted in June 2009, which provided the offshore wave forcing and data on the forereef, reef flat and lagoon that was required to drive and validate the numerical models. A detailed description of the study site, the field experiment, and

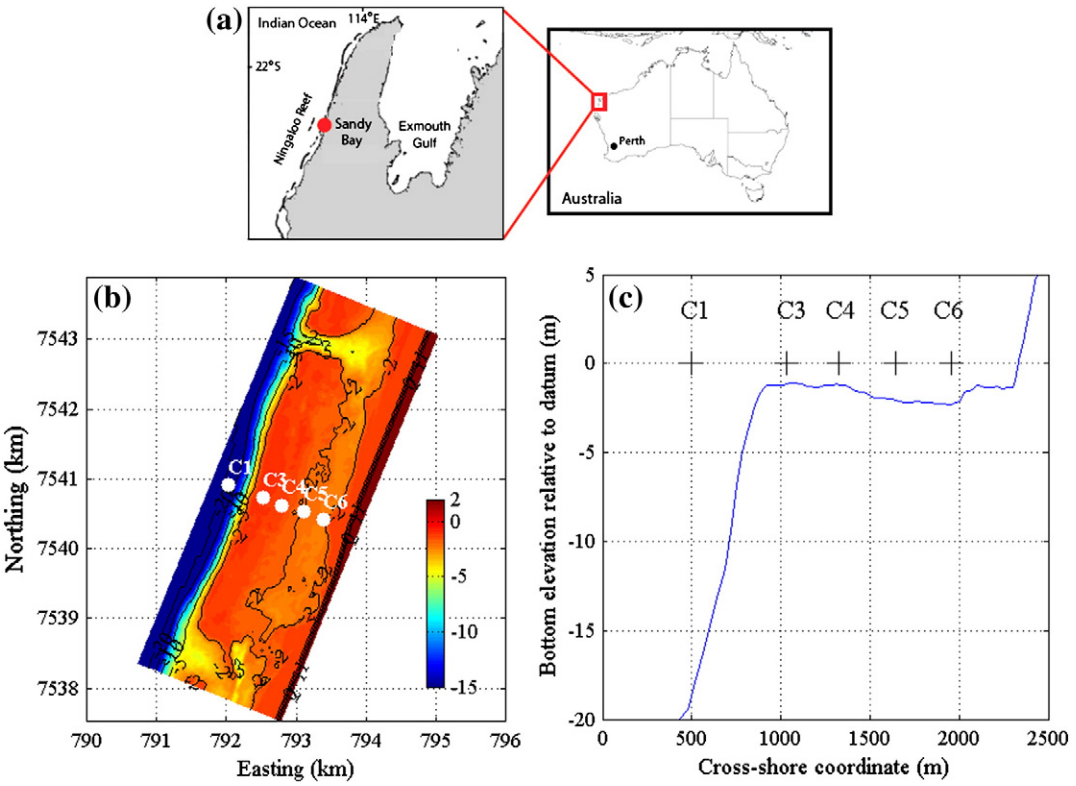

Fig. 1. (a) Location of Ningaloo Reef and the study site at Sandy Bay in Western Australia. (b) Plan view of the surveyed bottom contour elevations (relative to Australian Height Datum, equivalent to approximately mean sea level) with the instrument locations superimposed. (c) Cross-shore profile of the bathymetry along the main measurement transect with instrument locations shown.

results are discussed by Pomeroy et al. (2012), and only a brief summary is included here.

During the field experiment, a synchronized cross-shore and alongshore array of instruments was deployed (Fig. 1b). The present study focuses on the measurements obtained from the roughly perpendicular cross-shore transect (C1–C6) (Fig. 1c). Instrument C1 was deployed on the forereef slope, C3 and C4 were located on the reef flat, while C5 and C6 were located inside the lagoon behind the reef (C2 was a backup instrument collocated with C1 and was thus not used in the present paper). Based on the energy contained within the short wave (0.04–0.2 Hz or 5–25 s) and IG wave bands (0.004–0.04 Hz or 25–250 s), the short and IG wave heights $H_{rms,sw}$ and $H_{rms,IG}$ at all five instrument locations (Fig. 2e–f) were computed. The tidal or mean water level variation was obtained from the low-passed surface elevation signal below 0.004 Hz. This signal was demeaned over the measurement period which causes the instrument zero level to be at a higher vertical datum level than mean sea level since wave set-up variations are still included. This was corrected for by first computing the linear least-squares regression between the residual water level (i.e., the difference between the water level measured at each station on the reef and that measured at C1 where setup/setdown is assumed negligible) and the offshore wave power (proportional to $H_s^2T_p$). The records on the reef (C3–C6) were then corrected for the offset water level (based on the value at zero wave power), which amounted to a shift of about 0.08 m.

On the forereef at C1, the short waves overwhelmingly dominated over the IG waves (Fig. 2b). In contrast, on the seaward edge of the reef (C3), the short wave heights were substantially reduced and were comparable to the IG wave heights (Fig. 2c). At this location, both wave signals appeared in-phase with the tidal fluctuations, an observation that is discussed further in Section 5. The short and IG wave heights decreased across the reef (C4) and lagoon (C5 and C6)

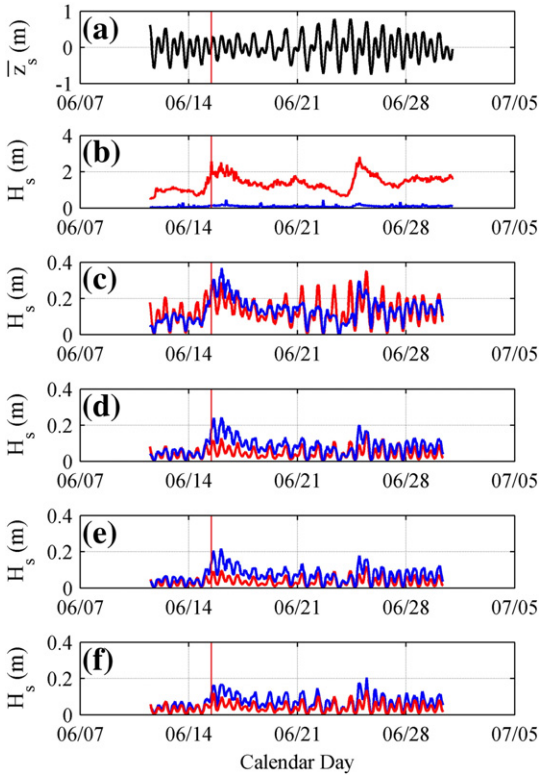

Fig. 2. (a) Time series of the mean water level (tide) measured on the forereef at C1. Root-mean-square wave heights for the infragravity wave band $H_{rms,IG}$ (blue) and short wave band $H_{rms,sw}$ (red) measured across the reef at (b) C1, (c) C3, (d) C4, (e) C5 and (f) C6. The vertical red lines denote the period of the peak swell event simulated on June 15 at 11:00.

with the short wave heights decaying more rapidly across the reef than the IG wave heights (Fig. 2d–f). A general increase in wave heights (short wave and IG) on the reef was observed during the two swell events that occurred around June 15 and June 25.

3. Numerical modeling

3.1. Model description

The numerical model used was XBeach (see Roelvink et al., 2009 for a complete description of the equations), which solves the coupled time-dependent 2DH (horizontal) equations of wave action propagation and dissipation (on the scale of the wave groups), and the 2DH equations of conservation of mass and momentum (for IG and mean surface elevation and currents). The model was forced by varying (spectral) wave and flow boundary conditions. The main innovation over previous steady (shortwave-averaged) wave-driven models is its non-stationary wave driver that incorporates directional spreading.

In XBeach, variations in radiation stresses derived from the short wave groups force IG wave motions within the model. The model thus includes the dynamics responsible for IG wave generation, propagation and decay. The model also solves the 2DH sediment transport equations and morphological changes, but these processes are not considered herein. This modeling approach (treating the short waves and IG waves separately with coupling) is designed to predict the bulk of the hydrodynamic variability present in nearshore systems, without the burden of the computational expense needed for the computation of the short wave shape and the dynamics of individual short waves. This makes 2DH simulations feasible for large domains of several square kilometers and for events lasting several days. XBeach has hitherto been successfully applied to predict the erosion of dune coasts (Roelvink et al., 2009) and the deformation of sandy barrier islands due to erosion and overwash under hurricane forcing (Lindemer et al., 2010; McCall et al., 2010), but has yet to be applied to reefs.

The only relevant change in the version that was applied here was the inclusion of an additional term in the wave action balance to account for bottom friction dissipation D_f of the short waves. Such bottom friction has been shown to play an important or even dominant role in reef environments (e.g., Lowe et al., 2005). The wave action equation for the short waves was thus modeled as:

$$\frac{\partial A}{\partial t}+\frac{\partial c_x A}{\partial x}+\frac{\partial c_y A}{\partial y}+\frac{\partial c_\theta A}{\partial \theta}=-\frac{D_b}{\sigma}-\frac{D_f}{\sigma} \tag{1}$$

where A is the wave action, c_x, c_y and c_θ are the propagation speeds in 2D horizontal and directional space (refraction), D_b is the rate of dissipation due to wave breaking and σ is the representative radian wave frequency (defined based on the mean period T_{m01} — see below). Wave dissipation due to breaking in Eq. (1) was modeled using Roelvink's (1993) breaker formulation with a breaker coefficient of $\gamma=0.55$. The rate of bottom friction dissipation D_f was modeled as (e.g., Jonsson, 1966):

$$D_f=\frac{2}{3}\rho\pi f_w\left(\frac{\pi H}{T_{m01}\sinh kh}\right)^3. \tag{2}$$

Here f_w is the short-wave friction coefficient, T_{m01} is the mean period defined by the first- and zeroth moments of the wave spectrum, and h is the water depth. In Eq. (2), H is the instantaneous root-mean-squared wave height defined as twice the value of the amplitude of the wave group envelope at a given time, which can be calculated from the wave action A (see Roelvink et al., 2009).

The momentum equations used to compute the mean currents, as well as time-varying IG wave orbital velocities and surface elevations (see Roelvink et al., 2009 for the full equations), contain a friction term of the form, e.g. for the cross-shore component (Ruessink et al., 2001):

$$\tau_{bx}=c_f\rho U_E\sqrt{(1.16\ u_{rms})^2+\left(U_E^2+V_E^2\right)} \tag{3}$$

where U_E and V_E are the x–y (cross-shore, alongshore) Eulerian flow velocities, u_{rms} is the root-mean-squared (rms) near-bottom short-wave orbital velocity (determined from the wave action A using linear wave theory), and c_f is the friction coefficient associated with both the mean currents and long period (IG) waves. We note that bed friction enters into the model system twice through the two coefficients f_w and c_f. Studies conducted on reefs (e.g. Lowe et al., 2007) indicate that f_w should be an order of magnitude (or more) larger than c_f due to the dependency of wave frictional dissipation rates on the frequency of the motion. In the present application, both friction coefficients were thus assumed to be independent.

3.2. Model application to Ningaloo Reef

XBeach was applied to the cross-shore transect (C1–C6) in 1D mode and to the whole study domain in 2DH mode (Fig. 1b and c). The bathymetry for both model domains was derived from hyperspectral imagery (HyMap) and processed by Curtin University (Klonowski et al., 2010) with a 3.5 m pixel resolution and <10% vertical depth error for depths up to 8 m. Horizontally coarser (~20 m) but very accurate (<5 cm depth error) multi-beam altimeter data were used for deeper regions (>8 m) within the model domain.

Wave forcing due to the time-varying short wave action variations and the associated bound IG waves at the offshore boundary were calculated from spectra derived from sea state parameters (wave height, peak period, mean direction and directional spreading) that were measured on the forereef at C1 (Fig. 3), following the approach by van Dongeren et al. (2003). In summary, this method generates time series of short wave surface elevations from data specified wave spectrum. The time series are then Hilbert-transformed to time variations of the short wave field envelope, which are finally converted to time-varying short wave action variations, i.e. the boundary condition for Eq. (1). The associated bound IG waves are computed from the spectral data using Herbers et al. (1994) theory. The mean surface elevation, interpolated from the hourly-averaged mean water level measured at C1, was added to the bound wave surface elevation and applied as the offshore boundary condition for the momentum equations. To increase the computational efficiency of the simulations (particularly in 2DH), a parallel MPI (Message Passing Interface) version of XBeach was used on an eight core Linux cluster.

Model output consisted of time series of the instantaneous short wave height H (calculated from the amplitude of the wave group envelope) and surface elevation z_s at each of the instrument locations (note that this surface elevation includes the effects of tide, mean short-wave induced set up and IG wave motions). The output was post-processed to compute the root-mean-square wave heights of the short wave ($H_{rms,sw}$) and the IG ($H_{rms,IG}$) frequency bands and compared against the wave heights measured in the field (Pomeroy et al., 2012).

4. Model results

4.1. One-dimensional simulations

The model was first run in 1D as this has traditionally been the focus of most phase-resolving numerical wave studies of IG wave dynamics in the nearshore, including laboratory reef prototypes (e.g., Nwogu and Demirbilek, 2010; Sheremet et al., 2011) due to

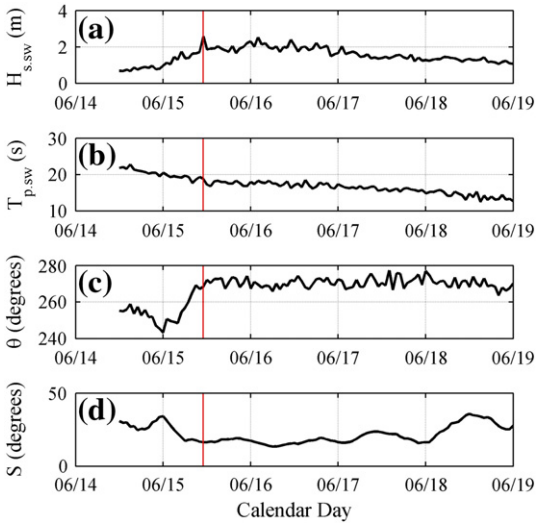

Fig. 3. Offshore short wave conditions at C1 with the peak swell event that was simulated indicated by the vertical red line. (a) Measured short wave height $H_{rms,sw}$, (b) peak short wave period $T_{p,sw}$, (c) mean short wave angle θ, (d) directional spreading S.

computation time constraints. The main purpose of this simulation was to identify the sensitivity of the model to the friction parameters f_w and c_f, as well as to identify the optimum values required to reproduce the key hydrodynamic processes (short waves, IG waves, and mean water levels) across the reef. The depth profile is shown in Fig. 1c and the presence of the shoreline at the downstream boundary requires the depth-integrated cross-shore transport to be zero at the shoreline by definition in 1D. The offshore boundary was initially prescribed with a single wave condition (H_s = ~2.5 m, T_p = ~19 s) corresponding to a peak swell event that occurred on June 15 around 11:00 (Fig. 3).

The 1D model was run for three different values of the short-wave friction coefficient f_w (0, 0.3, 0.6), while the current friction coefficient was held constant at $c_f = 0.1$ for all three cases. Note that the wave breaking dissipation D_b in Eq. (1) was modeled with the default free parameter value of $\gamma = 0.55$. The model results (not shown) were found to not be sensitive to variations of the parameter value within typical ranges (0.5–0.7) reported in wave transformation studies of reefs, which is consistent with Lowe et al. (2009b). The absence of short-wave friction ($f_w = 0$) resulted in an over prediction of the short wave heights across the reef (Fig. 4a). As f_w was increased, $H_{rms,sw}$ was more accurately reproduced across the reef, with very good agreement for $f_w = 0.6$ (Fig. 4a), especially considering the assumption of a spatially-uniform value for the friction coefficient whereas the reef would be spatially heterogeneous. The IG wave height transformation (Fig. 4b) and the mean water level prediction (Fig. 4c) also improved somewhat as f_w was increased; although both remained consistently over predicted. Note that because the observed wave action and mean water level are specified at the boundary, the model reproduces the measurements at C1 (Fig. 4a, b, e and f). However, the boundary condition for the IG waves is predicted from bound wave theory, which explains the difference between computed and observed IG wave heights at C1.

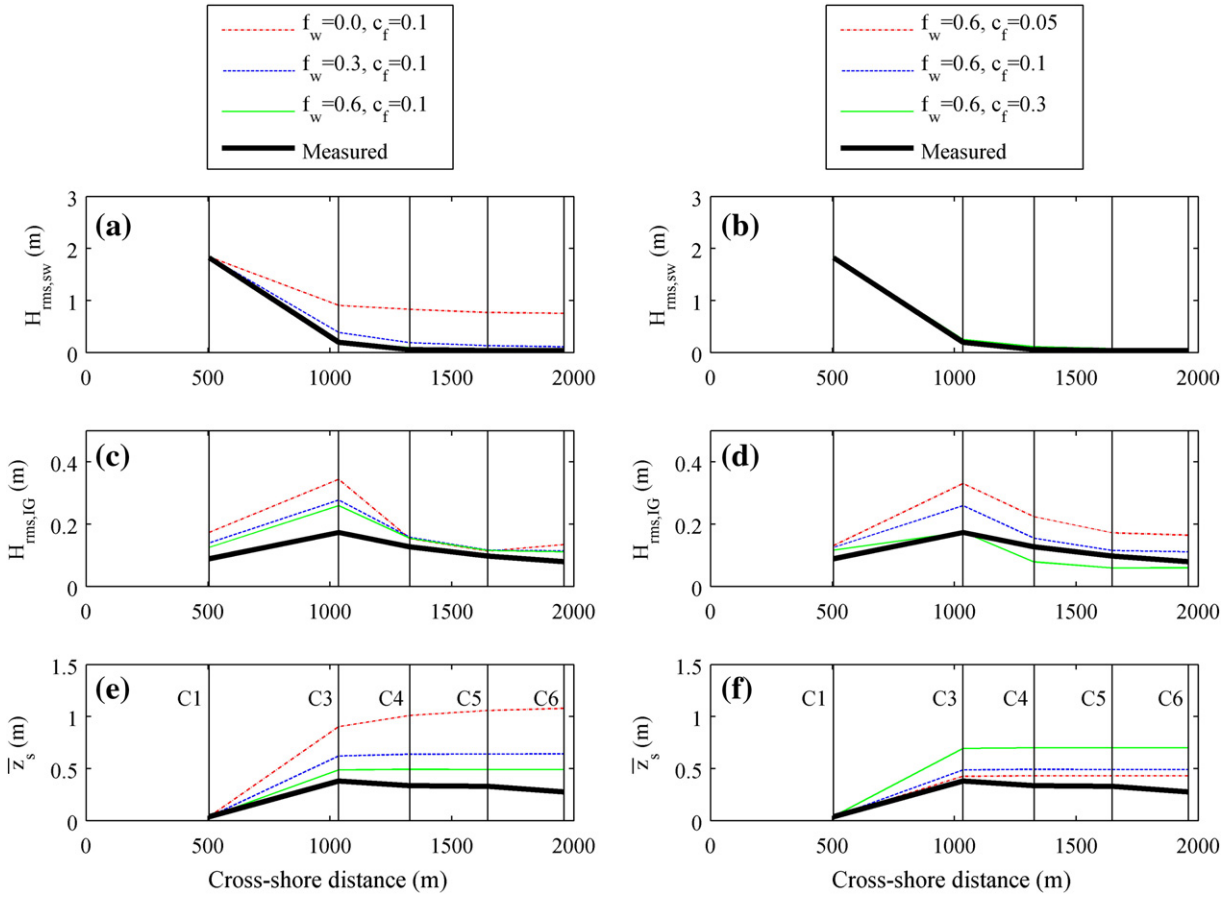

Fig. 4. 1D model simulations of the peak swell event (June 15 at 11:00). The left panels show the response to varying f_w, while the right panels show the response of varying c_f. (a,b) Short wave height $H_{rms,sw}$ transformation as a function of cross-shore distance, (c,d) IG wave height $H_{rms,IG}$, (e,f) mean water level (including tide).

A separate set of three simulations was conducted, this time using a constant short wave friction coefficient ($f_w = 0.6$) but for three values of the current friction coefficient c_f (0.05, 0.1, 0.3). For the higher friction coefficient value of $c_f = 0.3$, differences in the short wave heights $H_{rms,sw}$ were minimal (Fig. 4b, not visible in the plot). However, the IG wave heights $H_{rms,IG}$ improved, but these performance gains were at the expense of an increasing and significant over prediction in the mean water levels over the reef (Fig. 4e,f). The lower value of $c_f = 0.05$ produced the opposite effect, leading to a lower mean water level (which was more in agreement with the data); however, IG wave heights were significantly over predicted (Fig. 4d). The optimal combination of friction coefficients from these sensitivity tests was thus $f_w = 0.6$ and $c_f = 0.1$. While not a perfect match with the data, the 1D model captured the gradients in short waves, IG waves, and mean water levels observed across the reef moderately well.

The optimum friction coefficient values ($f_w = 0.6$, $c_f = 0.1$) were subsequently used to simulate the entire swell event from June 14 12:00 h to June 19 00:00 h (109 h in total) when wave conditions varied significantly. This allowed for an evaluation of the model performance under a wide range of incident short wave conditions. The swell event duration was represented in the model as a sequence of hourly sea states, from which the wave forcing was generated at the offshore boundary. The model tapered the time series for each sea state so that there was a smooth transition between them (see Van Dongeren et al., 2003). Good agreement was generally observed throughout the simulation and at all sites (Fig. 5). The model reproduced the spatial variability in wave heights across the reef, as well as temporal changes in the response to the varying offshore wave conditions and tidal variations. The short wave height predictions matched the data reasonably well (Fig. 5a–e), except for a small positive bias of a few centimeters. The IG wave heights were slightly under predicted (negative bias) at C1, but were generally in very good agreement for sites on the reef (Fig. 5f–j). The time series of the predicted mean water level residuals (the time-averaged difference between the observed water level on the reef and the observation at C1, $\overline{\Delta z_s} = \overline{z_s} - \overline{z_{s,C1}}$, thus describing wave setup) followed the observed residuals reasonably well, albeit that the model over predicts the observations by about 0.1 m (Fig. 5l–o) which is consistent with the over prediction shown in Fig. 4f. Note that at C1 the observed and predicted water levels rather than the residuals are shown (Fig. 5k)

A summary of the model skill (bias and the RMS error) for the short wave heights, IG heights and mean water level is shown in Fig. 6. Bias in the predicted short wave $H_{rms,sw}$ first increased positively from C1 to C3 to a value of +0.03 m and then decreased to nearly zero at the back of the reef, whereas the bias in the IG wave height at C1 $H_{rms,IG}$ was weakly negative (−0.04 m) and effectively zero on the reef. The bias in mean water level increased substantially from the offshore (C1) site to the four sites within the reef, where values were over predicted by roughly +0.1 m. The RMS errors show similar trends, with only small discrepancies in the short wave and IG wave heights of <0.03 m for sites on the reef (comparable to the accuracy of the field measurements, ~0.01 m); however, the 1D model still over predicted setup generated on the reef by +0.1–0.15 m.

4.2. Two-dimensional simulations

To investigate possible differences in the performance of the 1D and 2DH simulations, the model was then run in 2DH mode for the same single peak swell event and 5 day swell duration. The incident wave conditions were assumed to be alongshore uniform with the phase rotation of the wave energy and bound long waves over the boundary taken into account (enabling obliquely-incident wave groups and IG waves to be modeled). The sensitivity of the friction parameters (f_w and c_f) was re-evaluated to identify the optimum parameter combination in 2DH mode.

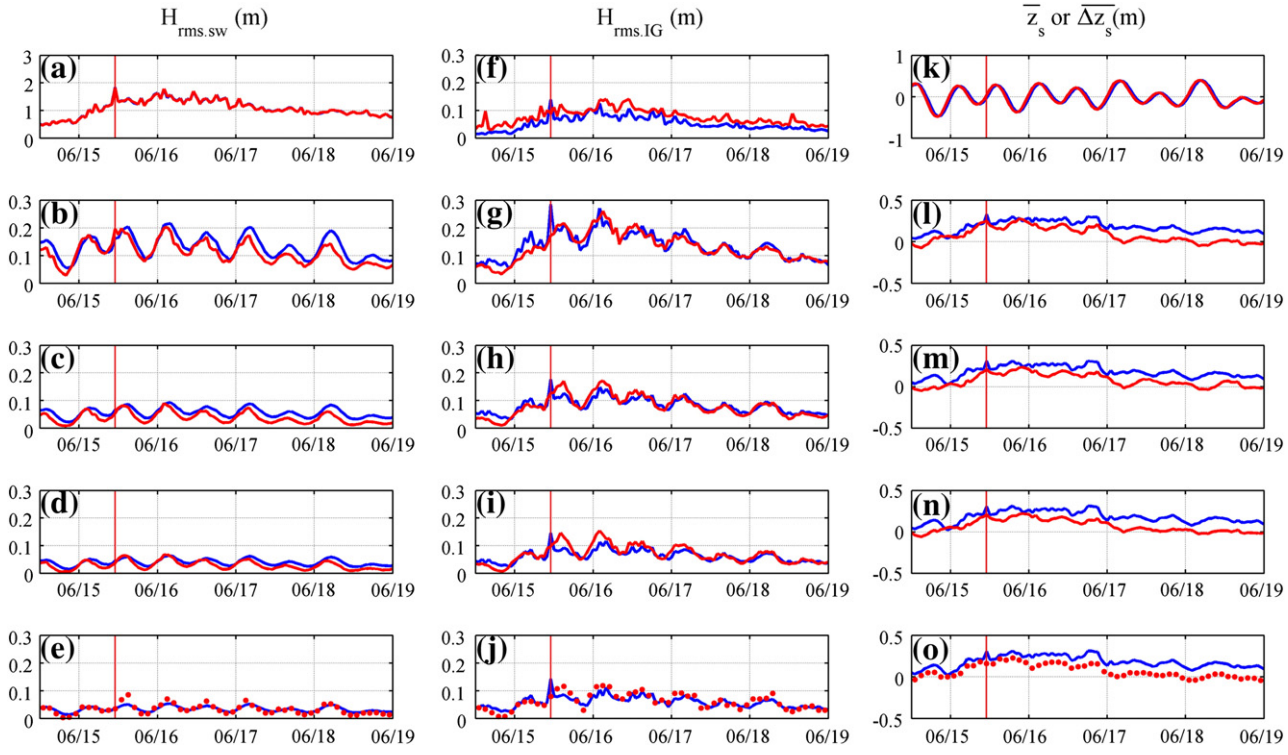

Fig. 5. Comparison between the 1D model results (blue) and measured data (red) for the duration of the ~5 day swell event. (a,f,k) are for instrument C1, (b,g.l) C3, (c,h,m) C4, (d,i, n) C5and (e,j,o) C6. The peak of the storm (simulated in this figure) is indicated by the red vertical line. Note the large reduction in vertical scale between C1 and the reef sites C3–C6.

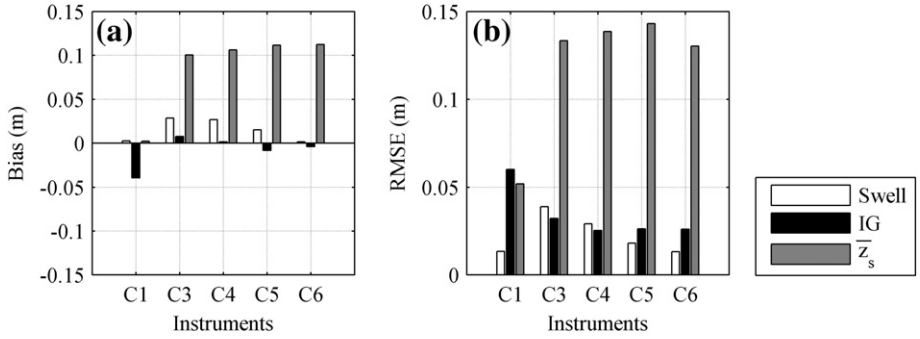

Fig. 6. Bias and RMS error from the 1D swell duration (~5 day) model results compared with the measured data at each site, based on the short wave heights, IG wave heights, and mean water levels.

The results at the peak swell event (Fig. 7) were somewhat different in the 2DH model, even when the same friction coefficients were used ($f_w = 0.6$, $c_f = 0.1$). In contrast to the 1D simulations, the IG wave heights across the reef were under predicted but the mean sea level was still slightly over predicted on the reef and in the lagoon (sources of the discrepancy in the response of the 1D and 2DH models are discussed in detail in Section 6.1). However, when c_f was decreased, better agreement was observed with the measured values for both the IG waves and mean sea level. Thus for the 2DH simulations, the optimum friction values were $f_w = 0.6$ and $c_f = 0.04$, with the c_f value (defined based on the depth-averaged flow) in this case being closer to values historically measured values on reefs, i.e. $c_f = 0.02$–0.05 (e.g., Lowe et al., 2008; Rosman and Hench, 2011). Fig. 8 shows two mean wave-driven circulation cells in the study area, with onshore flow over the reef diverging into more alongshore-dominated at the back of the reef and lagoon, before exiting the system via the two channels in the reef. These current patterns superimposed on the bathymetry are quite similar to those found on barred beaches (Reniers et al., 2004) and behind submerged breakwaters. These mean flow patterns are not represented in a 1D approach and ultimately influence both the mean sea level and wave (short and IG) across the reef (see discussion in Section 6.1).

As with the 1D model, the 2DH model was run with the optimum friction coefficients for the entire ~5 day swell event. Relative to the 1D results, some slight improvements in the 2DH results were observed for both short waves $H_{rms,sw}$ (Fig. 9a–e) as well as IG waves $H_{rms,IG}$ (Fig. 9f–j). However, the most significant improvement was made in the prediction of the mean water level residuals (wave setup) (Fig. 9l–o). In the 2DH model, the mean water level residuals were almost identical to the observations. The model performance statistics summarized in Fig. 10 highlight the overall performance gains in the 2DH model. The bias associated with the predicted mean sea level was most improved in the 2DH model, with bias

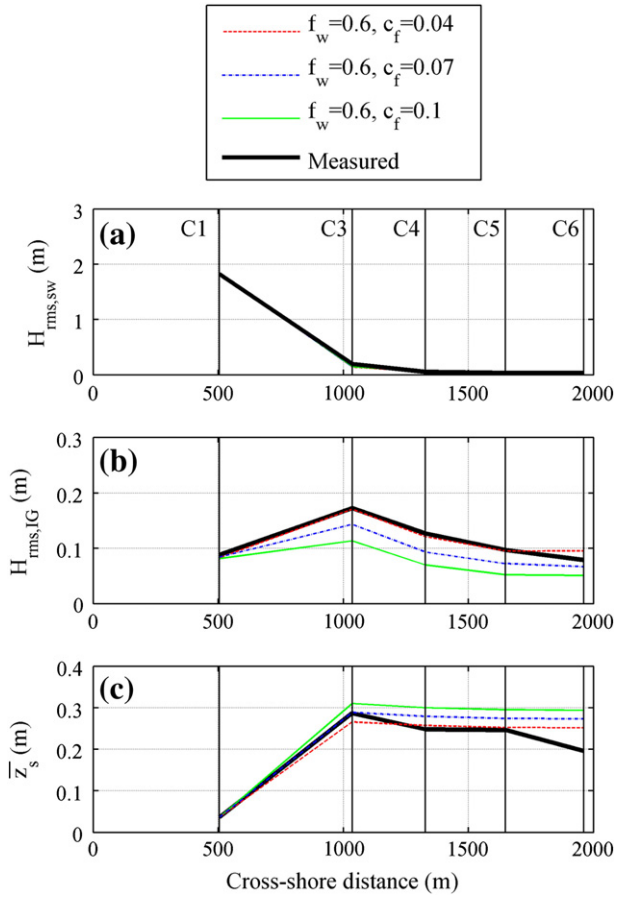

Fig. 7. 2DH model simulation results from the peak swell event (June 15 at 11:00), showing the influence of c_f with constant f_w on (a) short wave height transformation as a function of cross-shore distance (b), IG wave height and (c) mean water level.

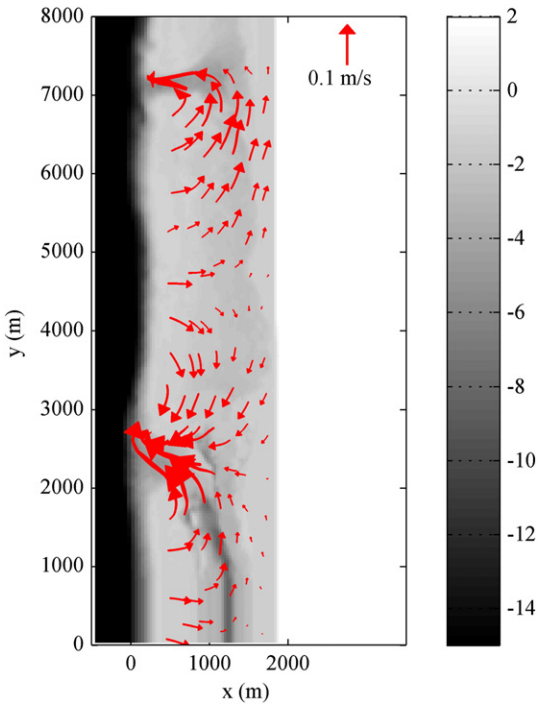

Fig. 8. Mean current velocity superimposed on the bathymetry. The colorbar denotes the mean water depth in meters.

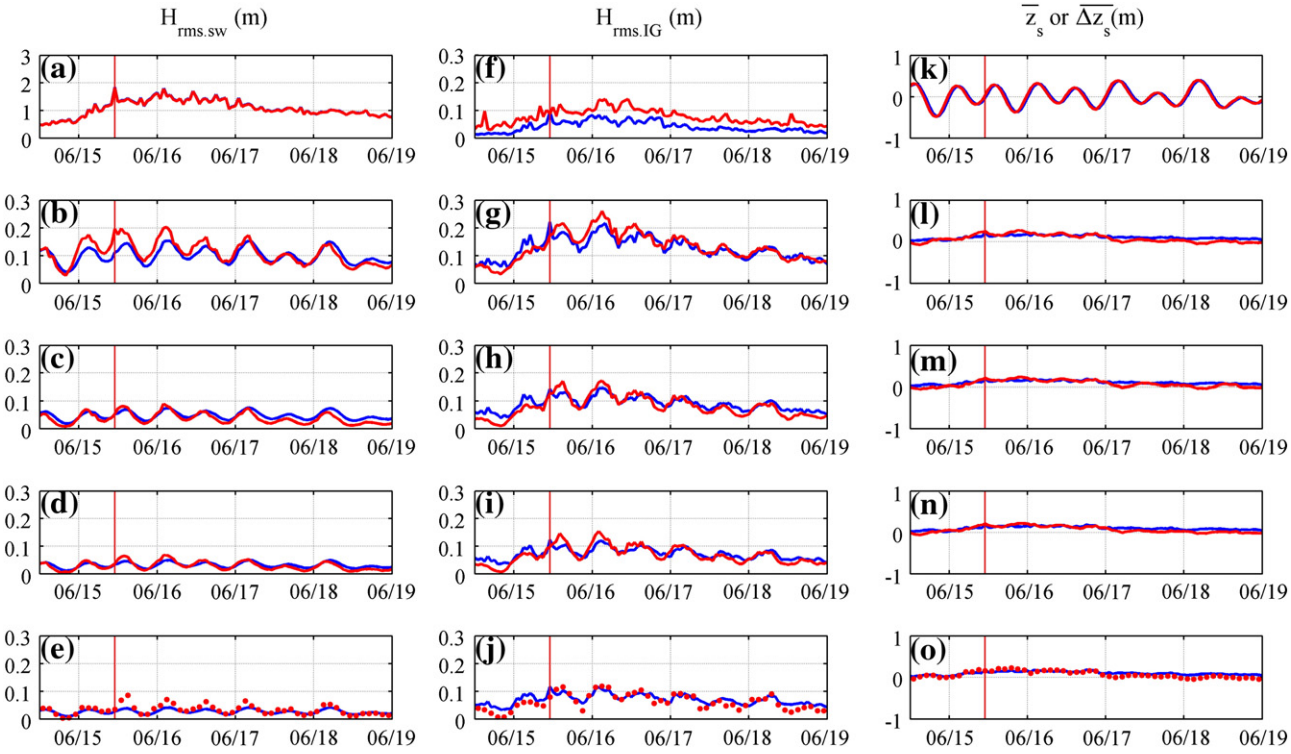

Fig. 9. Comparison between the 2DH model results (blue) and measured data (red) for the ~5 day duration of the swell event for $f_w = 0.6$ and $c_f = 0.04$. (a–c) are for instrument C1, (d–f) C3, (g–i) C3, (j–l) C4 and (m–n) C5. The peak of the storm is indicated by the red vertical line.

values of ~0.04 m observed across the reef and lagoon compared with the >0.1 m values predicted from the 1D model. In general, the discrepancies of the IG and short waves were also less than those predicted with the 1D model.

5. IG wave propagation, generation and dissipation

The optimum 2DH model configuration ($f_w = 0.6$, $c_f = 0.04$) was used to investigate the detailed dynamics of the IG wave motions across the reef. The focus of this analysis was to evaluate how the IG waves propagate across the reef (Section 5.1), the mechanisms responsible for their generation and dissipation (Section 5.2) and also to place these results in the context of the field observations reported in Pomeroy et al. (2012) using this much more highly-resolved model output. For this analysis, the model was forced by the wave conditions during the peak swell event (June 15, 11:00).

5.1. Propagation

The computed time series of the low frequency cross-shore (U) and alongshore (V) velocities were used to construct a 2DH map of the velocity variance ellipses using a Principal Component Analysis (PCA) (Emery and Thompson, 2001) (Fig. 11a), where the ellipses represent the major and minor axes of the IG flow variability. Consistent with the field observations, the size of the major axes (cross-shore) increases significantly near the reef crest and gradually decays towards shore. Importantly, the IG velocity variance ellipses are dominantly oriented towards shore (generally within a few degrees of the shore-normal direction), except near the channel edges where some refraction occurs. This indicates that the IG waves propagate primarily in the cross-shore direction, with only a minimal alongshore contribution.

To specifically identify the presence of edge waves, wavenumber-frequency (k_y-f) spectra (Huntley et al., 1981) were computed for an

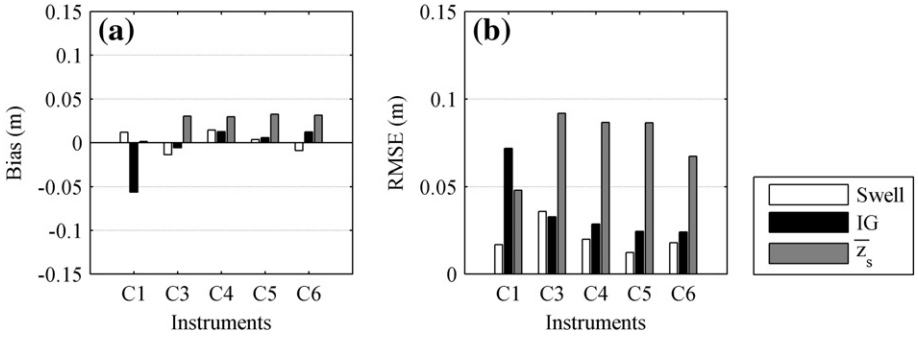

Fig. 10. Bias and RMS error of the 2DH swell event model results compared with the measured data at each site, based on the short wave heights, IG wave heights, and mean water levels.

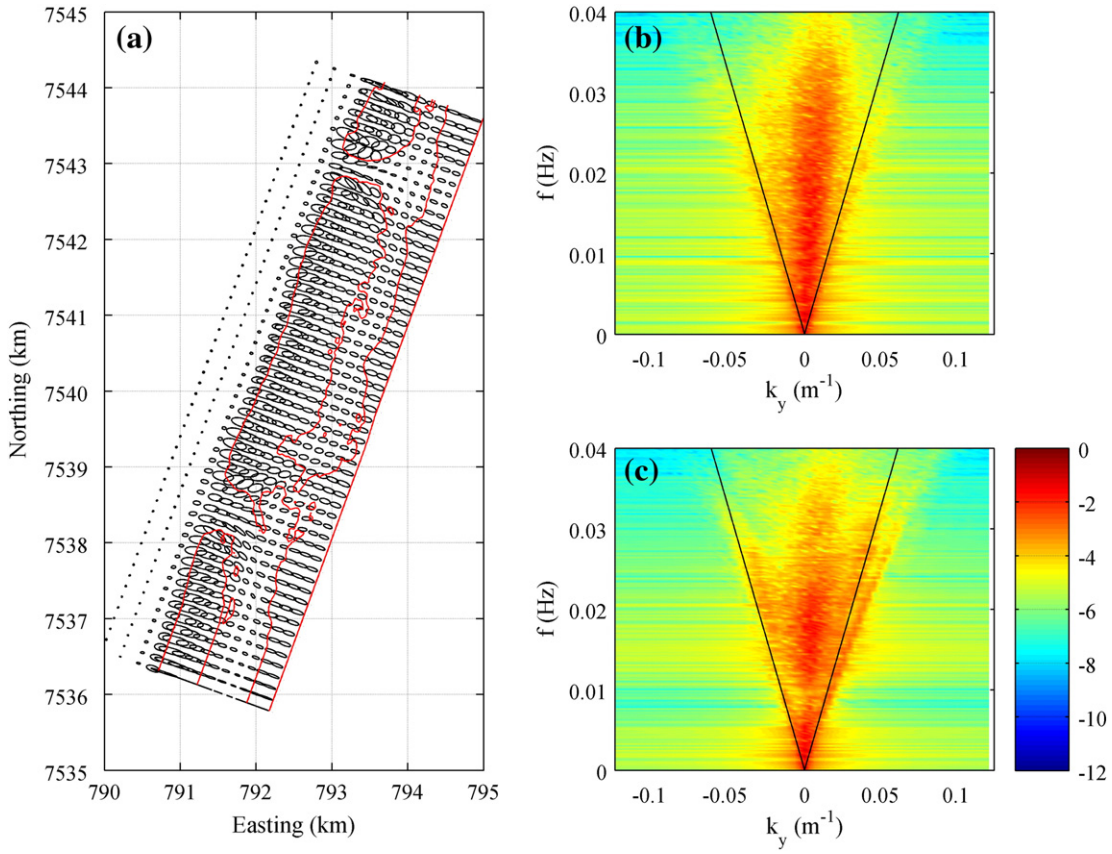

Fig. 11. (a) Principal component analysis of the velocities with the underlying bathymetry contours ($h=0$ and 2 m) indicated by the red lines; (b) k_y-f spectra on the reef flat ($x=1053$ m); (c) k_y-f spectra in the lagoon ($x=1663$ m). The shallow water dispersion curves based in Eq. (4) are indicated by the black lines with the energy density values denoted by the colorbar. The array length at both sites was 75 m.

alongshore transect of 75 m in length at two cross-shore locations, $x=1050$ m on the reef (Fig. 11b) and at $x=1660$ m in the lagoon (Fig. 11c). These results indicate that energy at both locations, IG energy is primarily located within a leaky wave region bounded by the shallow water wave dispersion curves

$$f = \sqrt{gh}\frac{k_y}{2\pi} \tag{4}$$

where f is the wave frequency and, for simplicity, h is taken is the local water depth. Only very minimal edge wave energy is present outside of these theoretical curves, thus also consistent with the dominant cross-shore orientation of the IG flow variance ellipses in Fig. 11a.

5.2. Generation

The model results showed that IG wave heights increased in size on the forereef and the surfzone between C1 and C3, while they decayed gradually across the reef flat. Pomeroy et al. (2012) showed with 1D XBeach model simulations that IG waves were generated in the surfzone by breakpoint generation (Symonds et al., 1982) rather than by bound wave growth in the shoaling zone (Battjes et al., 2004; Longuet-Higgins and Stewart, 1964). A cross-correlation analysis between the incident short wave envelope $|A(t)|$ at C1 with the IG wave time series at all locations across the model domain using the 2DH2D model (Fig. 12b) shows similar results to those using the 1D model (Pomeroy et al., 2012). Despite the directional spreading in 2DH, the results confirm that the IG wave propagation is dominantly onshore. In the offshore region, the correlation patterns show a dominant negative correlation between the short wave envelope and IG wave signal, characteristic of bound IG waves coupled to the short wave groups. A positive correlation then develops over the reef, with the development of a dynamic setup and a negative correlation propagating offshore from the breaking region, all consistent with the breakpoint forcing mechanism (e.g., Baldock et al., 2000; Symonds et al., 1982). In contrast with the 1D results, the value of the correlation coefficients is smaller due to the directional spreading in the short wave groups and the wave celerity over the reef is slightly smaller due to the lower setup over the reef depth.

5.3. Dissipation

Both the field observations (Fig. 2; see also Pomeroy et al., 2012) and model results displayed a strong positive correlation between changes in the IG wave heights over the reef and the mean water depth (tidal) variations. The tidal modulation of IG wave heights has also been observed previously on the inner shelf, seawards of the surf zone on sandy coasts (e.g., Okihiro and Guza, 1995; Thomson et al., 2006). Weak tidal modulation of IG waves has also been observed shoreward of the surf zone on beaches (Henderson et al., 2006; Reniers et al., 2002). To investigate the mechanisms responsible for the strong tidal modulation of the IG waves observed in present study (i.e., Fig. 9), simulations were conducted at two different water depth limits bounding the historical mean tidal range limits at this site, i.e. values of $+0.43$ m (high tide) and -0.43 m (low tide), both offshore values (without wave-induced setup). For each simulation the offshore wave boundary condition was held constant, and the model output across the reef (surface elevations and velocities) was analyzed to extract the incident (shoreward) and reflected (seaward) IG waves using the linear separation

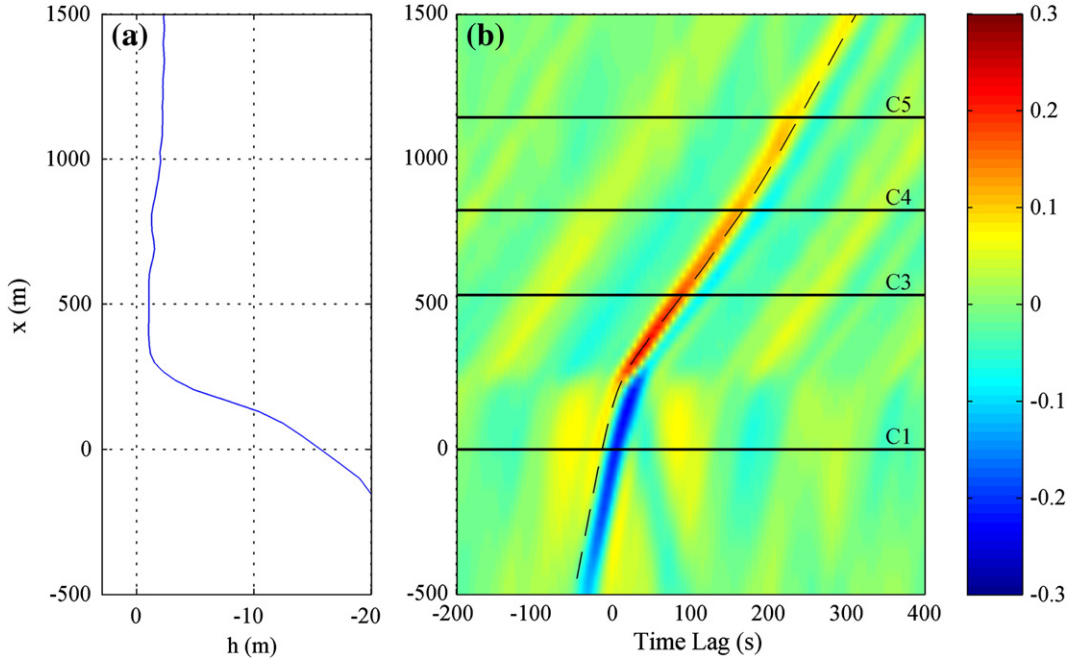

Fig. 12. (a) The Ningaloo Reef cross-shore bathymetry profile along the instrument array transect. (b) Cross-correlation of the amplitude of the short wave envelope $|A(t)|$ at C1 with the shoreward IG wave time series η_{IG} at each instrument location with the results from XBeach forced by the swell conditions of 16 June, 05:00. The dotted line denotes the theoretical linear shallow water speed trajectory obtained by integration of the cross-shore depth profile (including wave setup).

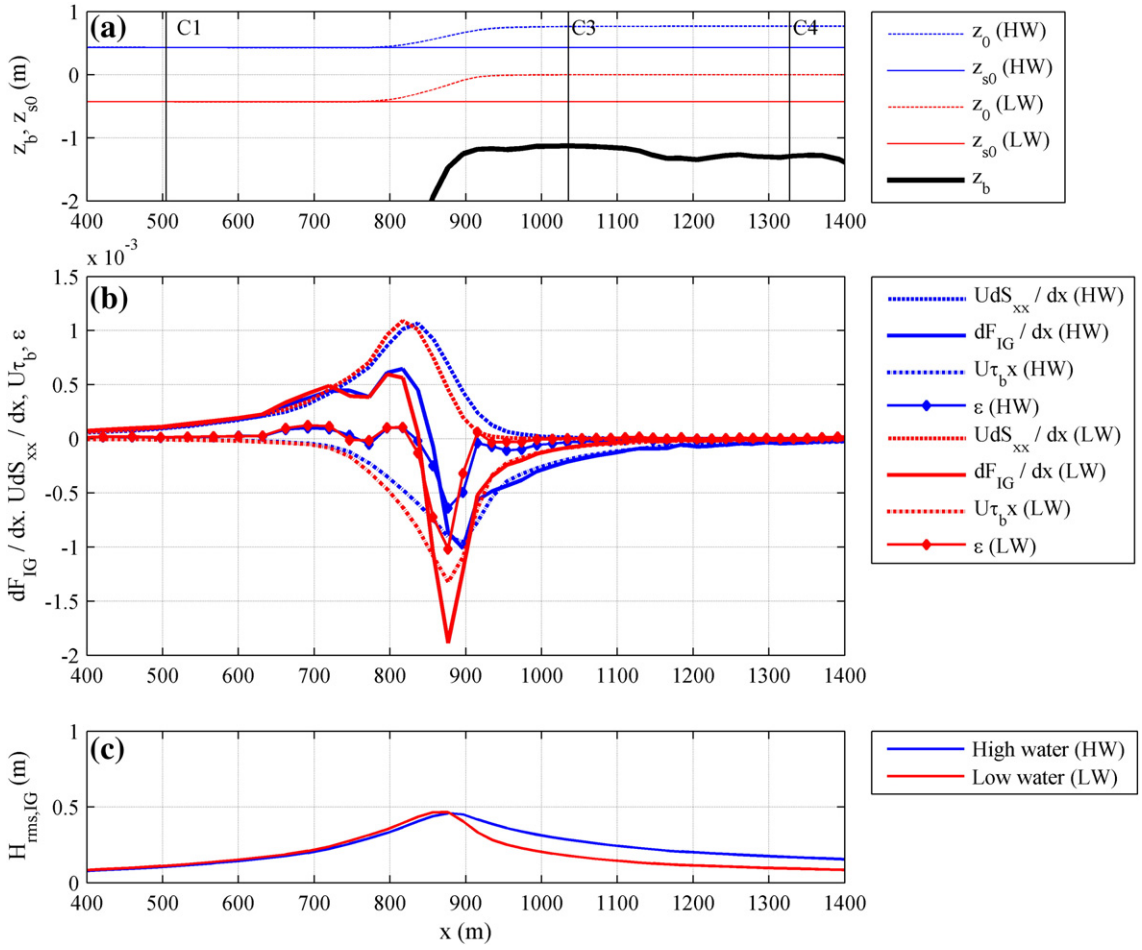

Fig. 13. (a) Bathymetry (z_b) and water levels for reference where z_{s0} is the original water level and z_0 is the water level inclusive of setup; (b) IG wave flux gradients dF_{IG}/dx (red solid and blue solid for higher and lower water level respectively); short wave work term $\langle UdS_{xx}/dx \rangle$ (dashed lines); bottom friction sink term $\langle U\tau_{b,x} \rangle$ (dash-dotted line); IG wave breaking dissipation ε (dotted); (c) incoming IG wave heights $H_{rms,IG}$.

technique of Guza et al. (1984), i.e. the (small) seaward reflected components were removed for the purpose of this analysis. For the incoming wave component, the energy balance for the IG waves was quantified over the cross-reef transect as (Phillips, 1977; Schaeffer, 1993):

$$\frac{dF_{IG}}{dx} = \left\langle U\frac{dS_{xx}}{dx}\right\rangle + \left\langle U\tau_{b,x}\right\rangle + \varepsilon. \quad (5)$$

Here F_{IG} is the IG wave energy flux of the incoming wave, U is the Lagrangian flow velocity that includes the incoming IG waves and mean currents, dS_{xx}/dx is the radiation stress gradient, $\tau_{b,x}$ is the bottom stress and ε represents IG wave bore dissipation (but includes also residuals due to nonlinearities, numerical inaccuracy, etc.). Eq. (5) implies that IG energy across the reef can be either generated or lost due to the work done by the short waves on the long waves (first term, right hand side), and that energy may also be lost due to bottom friction dissipation (second term, right hand side) and IG bore dissipation (third term, right hand side).

The short wave-induced set up for the two water depths was about 0.4 m. (Fig. 13a, dashed lines). The IG energy balances for both cases (Fig. 13b) revealed that the energy flux gradients dF_{IG}/dx (solid lines) were positive where the short waves were shoaling and breaking (i.e., $x<850$ m), as a result of the short waves transferring energy to the IG waves (dashed lines). At higher tide, there is a slight shoreward shift in the peak of the work done by the short waves $\langle UdS_{xx}/dx\rangle$ (dashed lines), corresponding to a shift of the mean surf zone position; however, the magnitude of the work done is not significantly affected.

From the reef crest shoreward ($x>850$ m), the IG energy flux gradients reversed signs resulting in a net dissipation of energy towards shore. This sign reversal coincided with locally large negative values of the IG wave bore dissipation term ε, which is otherwise near zero everywhere else. This could be due to local IG wave breaking which occurs when the IG wave height to water depth ratio becomes large. From the results for a hypothetical case of no friction (not shown), the model results displayed significant IG wave bore formation across the reef flat and lagoon and much more associated dissipation. With friction turned on, the IG waves did not steepen up to form bores over the flat and in the lagoon (i.e., for $x>900$ m).

The two tidal level scenarios show significant differences in the magnitude of work done by bottom friction dissipation $\langle U\tau_{b,x}\rangle$ (Fig. 13b). Near the reef crest ($750<x<900$ m), rates of IG bottom friction dissipation are higher for the lower water depth case, as a result of the increase in the IG wave velocities U in the shallower water column for the same IG energy flux (Fig. 13b,c). Consequently, at higher water depths, more IG energy flux persists over the reef flat and lagoon ($x>900$ m) which is balanced by a larger bottom friction dissipation (as a result of the higher IG fluxes in this region). This suggests that tidal variability in the IG wave heights on the reef is not due to significant differences in the rate of IG generation in the surf zone, but instead is primarily due to the tidal modulation in the rates of frictional dissipation due to the changing depth of the water column.

6. Discussion

6.1. Model performance: 1D versus 2D

XBeach was found to predict the range of important hydrodynamic processes across a complex reef-lagoon system with relatively good accuracy in both the 1D and 2DH modes for different sets of bottom friction parameter values. In both modes, the same optimum value for the short wave friction coefficient f_w was found. However, the current/IG friction coefficient c_f was reduced by approximately 50% in the 2DH case to most accurately predict both the IG wave transformation across the reef and the mean water level (setup) variations.

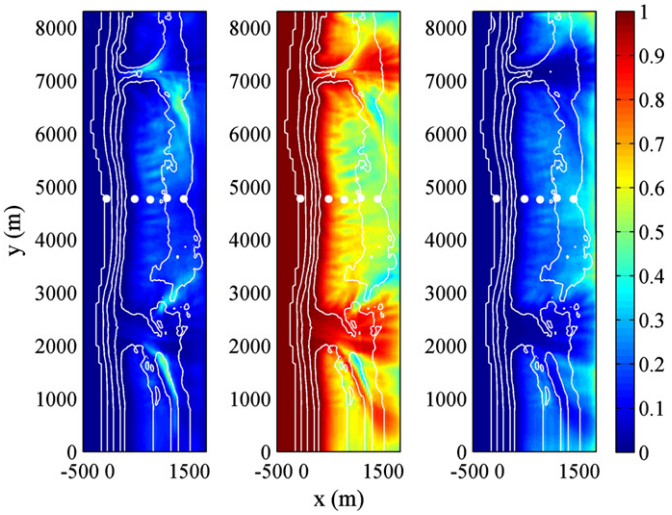

Fig. 14. The fraction (denoted by the colorbar) of total bed shear stress driven by (a) the mean currents (b) short waves (c) and IG waves, averaged over the duration of the 2DH model during the peak swell event. The white dots indicate the locations of the instruments used in the field experiment.

The physical reason responsible for the differences between the 1D and 2DH response can be explained by differences in the mass and momentum balances that are established across the reef under these configurations, for two primary reasons.

First, in 1D mode the short-wave action only forces the shore-normal radiation stress S_{xx}, with other components of the tensor being zero. This overestimates the generation of normally incident IG waves relative to the 2DH directionally-spread case (compare Fig. 4d to Fig. 7d for $c_f=0.1$). This excess IG wave energy thus needs to be balanced by higher rates of bottom friction dissipation. However, an increase in c_f also causes larger mean water level (wave setup) gradients, hence explaining the opposing trends found in Fig. 4 (right hand column). Thus the optimal value of c_f is the one that minimizes the model-data mismatch of both the IG wave heights and set up. In the 2DH mode, short wave energy is also transformed into lateral currents (Fig. 8), and hence less IG wave energy is generated. This requires less dissipation to match the data and thus a lower value of c_f, which causes less setup (compare Fig. 4c to Fig. 7f). Second, with the inherent assumption of zero (Lagrangian) cross-reef transport in the 1D model due to the closed shoreline and lateral boundaries, the depth-averaged mean Eulerian flow balances the wave-induced mass flux (i.e., Stokes drift) (Svendsen, 1984). This undertow produces a seaward-directed mean bottom stresses that leads to enhanced wave setup generated on the reef. In 2DH mode, there is a significant shoreward-directed Eulerian mean flow over the reef (see current vectors in Fig. 8) which instead leads to a shoreward-directed mean bottom stress; this momentum 'sink' significantly reduces wave setup over the reef flat and lagoon (Lowe et al., 2009a). Alternatively, for the 1D case it may also be possible to implement a shoreward outflow boundary (thereby reducing wave setup across the reef) by parameterizing the momentum balance in the lagoon and channel regions that is neglected in 1D, i.e. following the approach proposed by Lowe et al (2009a); however, such an empirical approach is not considered in the present study.

We finally note that the absence of a spatially-varying bed roughness coefficient in this implementation of the model may account for the slight over prediction of the mean water level at the nearshore (lagoon) measurement station where roughness is generally less than over the reef flat. Model performance could perhaps be further enhanced by incorporating detailed maps of bottom roughness as, e.g., inferred from habitat maps.

6.2. IG wave dynamics over fringing reefs

The results from this study highlight the importance of bottom friction to IG wave dynamics over coral reefs, which differs significantly from sandy coasts. First, the wide (>1 km) flat lagoon is not conducive to edge wave trapping that was commonly observed on beaches, which results in predominantly cross-shore propagating IG modes. Second, the influence of bed friction in this study also suggests that IG wave dissipation by bottom friction, as a result of the large physical roughness, is more dominant on reef systems in contradiction to beaches where nonlinear energy losses of IG waves can be dominant (e.g., Henderson et al., 2006; Thomson et al., 2006). In particular, the friction coefficients c_f for IG wave dissipation (for the 2DH case) were also very similar to the coefficients estimated directly from the field data (Pomeroy et al., 2012). The cross-shore IG energy budget analysis (Fig. 11) showed that the bottom friction term and IG wave energy flux gradients were roughly in balance over the reef flat and lagoon. This implies that dissipation due to other mechanisms such as steepness-induced (bore) dissipation of IG waves is only locally (shoreward of the breakpoint) important. In other words, bottom friction dissipation prevents wave steepening and steepness-induced breaking of the IG waves that have been observed on sandy beaches (De Bakker and Ruessink, in press; Ruessink et al., 1998; Senechal et al., 2001).

Moreover, the results from this study emphasize the importance of IG waves to coral reef systems, which compared to other hydrodynamic processes (e.g., short wave transformation and mean wave-driven currents), have frequently been neglected. The spatial importance of IG waves versus other processes (i.e., short waves and mean currents) is illustrated by computing the percentage of the total bed stress explained by each process, shown in Fig. 14 during the peak swell event. The components of the bed shear stress are computed for the mean currents τ_c, IG waves τ_{IG}, and swell waves τ_{sw}, diagnostically as

$$\begin{aligned}\tau_c &= \rho\ c_f\left(\bar{U}_E{}^2 + \bar{V}_E{}^2\right)\\ \tau_{IG} &= \rho\ c_f\left(\overline{U_E^2} - \bar{U}_E{}^2 + \overline{V_E{}^2} - \bar{V}_E{}^2\right)\\ \tau_{sw} &= \frac{1}{2}\rho\ f_w u_{rms,sw}^2\end{aligned} \tag{6}$$

where for the infragravity-wave component only the time-varying components of the Eulerian velocities (U_E,V_E) are taken into account.

The results show that mean currents generally account for less than 20% of the bottom shear stresses that occur over the reef and throughout most of the lagoon (Fig. 14a). On the forereef and near the reef crest (offshore of the surf zone), short waves account for almost 100% of the shear stresses observed (Fig. 14b). However, the influence of the short waves dramatically decreases across the reef flat and within the lagoon, typically accounting for <40% of the shear stresses in the lagoon. Notably, the contribution of IG waves to the total shear stresses gradually increases across the reef towards the lagoon and ultimately makes the dominant contribution (generally accounting for up to 50% of the shear stress in the lagoon) (Fig. 14c). Such spatial distribution patterns of bed stresses have numerous applications to reef systems, which in addition to controlling sediment transport patterns (e.g., Storlazzi et al. 2011) also control rates of mass-transfer limited nutrient uptake by coral reef communities that functionally depends on the bed stresses (e.g., Zhang et al., 2011) as well as the hydrodynamic forces imposed on reef organisms (e.g., Grigg, 1998). Moreover, the results indicate that IG waves should account for much of the shoreline run-up that occurs on reef-protected sandy beaches (Nwogu and Demirbilek, 2010); hence, these must be included to properly assess the longer-term morphological development of reef-fringed coastlines. Overall, from the results it is clear that IG waves play an important role in the hydrodynamics throughout fringing reef systems, especially within the lagoon and shoreline regions where they can eventually dominate over short waves and currents. It is thus critical to incorporate IG waves into the context of a range of morphological and ecological process-studies of reefs, which have historically almost exclusively focused on the only the role of mean currents and short waves.

7. Conclusions

This study demonstrates that the nearshore circulation model XBeach with an unsteady wave driver, initially developed for sandy coast applications, can be used with good skill to predict all of the key hydrodynamic processes across fringing reef systems (including important IG wave dynamics). The only modification to the model equations was the addition of a bottom friction dissipation term in the short wave energy balance, and the calibration of two bed friction coefficients (one for short waves and one for (un)steady currents) to higher values than commonly applied to sandy coast environments. The parameter associated with short wave dissipation (f_w) was an order of magnitude higher than the parameter c_f associated with unsteady currents (which includes IG waves), consistent with the frequency dependent response of the bottom dissipation rates (Lowe et al., 2007). The strict shore-normal forcing in the 1D model resulted in larger IG wave generation and required higher wave bottom friction coefficients c_f to reproduce the field observations. Also, due to these higher friction coefficients, wave setup was significantly over predicted in 1D and the variability lagged the observed phasing. In 2DH, directionally-spread forcing caused significant cross- and alongshore mean flows leading to lower mean water levels (wave setup) over the reef and less IG wave generation. As a result, lower current/IG wave coefficients c_f were required in the 2DH modeling, with these values much more closely aligning with field data and estimates from other coral reef systems.

IG waves were found to propagate with a dominantly cross-shore orientation across the reef, with the majority of the energy contained within the leaky region of the frequency-wave number spectra. Some weak energy patterns consistent with the presence of edge waves were observed, but their overall contribution to the IG motions was minimal. The IG wave height on the reef was strongly dependent upon the water depth over the reef. Results from the IG wave energy balance indicated that these IG tidal modulations were primarily due to differences in rates of friction-related IG wave damping at the different depths. IG wave energy accounted for a significant proportion of the bed shear stresses observed in the lagoon, whereas the short waves dominated on the forereef and reef crest. These finding indicate that the dynamics of IG waves are important across fringing reefs and their lagoons, and hence are likely to have a significant impact on a wide range of reef processes, both physical and biological, that operate within these systems.

Acknowledgments

This research was sponsored by Deltares Strategic Research 1202362 and the UNESCO-IHE DUPC MSc publication fund. RJL acknowledges funding provided by an Australian Research Council Discovery grant (DP0770094) and an Australian Research Council Future Fellowship (FT110100201), as well as support from a CSIRO Flagship Collaboration Fund grant.

References

Atkinson, M.J., Falter, J.L., 2003. Coral reefs. In: Black, K.P., Shimmield, G.B. (Eds.), Biogeochemistry of Marine Systems. CRC Press, Boca Raton, Florida, pp. 40–64.

Baldock, T.E., Huntley, D.A., Bird, P.A.D., O'Hare, T., Bullock, G.N., 2000. Breakpoint generated surf beat induced by bichromatic wave groups. Coastal Engineering (ISSN: 0378-3839) 39 (2–4), 213–242 http://dx.doi.org/10.1016/S0378-3839(99)00061-7.

Battjes, J.A., Janssen, J.P.F.M., 1978. Energy loss and set-up due to breaking of random waves. Proc. 16th Int. Conf. Coastal Eng., ASCE, pp. 569–587.
Battjes, J.A., Bakkenes, H.J., Janssen, T.T., Van Dongeren, A.R., 2004. Shoaling of subharmonic gravity waves. Journal of Geophysical Research 109 (C2), C02009 http://dx.doi.org/10.1029/2003JC001863.
Brander, R.W., Kench, P.S., Hart, D., 2004. Spatial and temporal variations in wave characteristics across a reef platform, Warraber Island, Torres Strait, Australia. Marine Geology 207, 169–184.
Darwin, C.R., 1842. The structure and distribution of coral reefs. Being the First Part of the Geology of the Voyage of the Beagle, Under the Command of Capt. Fitzroy, R.N. During the Years 1832 to 1836. Smith Elder and Co., London. (http://darwin-online.org.uk/EditorialIntroductions/Chancellor_CoralReefs.html).
De Bakker, A.T.M., Ruessink, B.G., in press. Infragravity-wave dynamics on a highenergy, gently sloping beach. Proc. International Conference on Coastal Engineering, Santander, Spain.
Emery, K.O., Kuhn, G.G., 1982. Sea cliffs: their processes, profiles, and classification. Geological Society of America Bulletin 93 (7), 644–654.
Emery, W.J., Thompson, R.E., 2001. Data Analysis Methods in Physical Oceanography. Elsevier, New York . (650 pp.).
Falter, J.L., Atkinson, M.J., et al., 2004. Mass transfer limitation of nutrient uptake by a wave-dominated reef flat community. Limnology and Oceanography 49, 1820–1831.
Gerritsen, F., 1980. Wave attenuation and wave set-up on a coastal reef. Proc. 17th Int.Conf. Coastal Eng., ASCE, pp. 444–461.
Gourlay, M.R., Colleter, G., 2005. Wave-generated flow on coral reefs—an analysis for two-dimensional horizontal reef-tops with steep faces. Coastal Engineering 52 (4), 353–387.
Grigg, R.W., 1998. Holocene coral reef accretion in Hawaii: a function of wave exposure and sea level history. Coral Reefs 17 (3), 263–272.
Guza, R.T., Thornton, E.B., Holman, R.A., 1984. Swash on Steep and Shallow Beaches, Paper Presented at 19th Coastal Engineering Conference. Am. Soc. of Civ. Eng., Houston, Tex.
Hardy, T.A., Young, I.R., 1996. Field study of wave attenuation on an offshore coral reef. Journal of Geophysical Research, Oceans 101 (C6), 14311–14326.
Hearn, C.J., 1999. Wave-breaking hydrodynamics within coral reef systems and the effect of changing relative sea level. Journal of Geophysical Research 104 (C12), 30,007–30,019 http://dx.doi.org/10.1029/1999JC900262.
Hench, J.L., Leichter, J.J., Monismith, S.G., 2008. Episodic circulation and exchange in a wave-driven coral reef and lagoon system. Limnology and Oceanography 53 (6), 2681–2694.
Henderson, S.M., Guza, R.T., Elgar, S., Herbers, T.H.C., Bowen, A.J., 2006. Nonlinear generation and loss of infragravity wave energy. Journal of Geophysical Research 111, C12007 http://dx.doi.org/10.1029/2006JC003539.
Herbers, T.H.C., Elgar, S., Guza, R.T., 1994. Infragravity-frequency (0.005–0.05 Hz) motions on the shelf: I. Forced waves. Journal of Physical Oceanography 24, 917–927.
Huntley, D.A., Guza, R.T., Thornton, E.B., 1981. Field observations of surf beat .1. Progressive edge waves. Journal of Geophysical Research, Oceans 86 (7), 6451–6466.
Jago, O.K., Kench, P.S., Brander, R.W., 2007. Field observations of wave-driven water-level gradients across a coral reef flat. Journal of Geophysical Research, Oceans 112 (C6).
Jonsson, I.G., 1966. Wave Boundary Layers and Friction Factors, Paper Presented at Tenth Conference on Coastal Engineering. ASCE, Tokyo, Japan.
Kench, P.S., Brander, R.W., 2006. Wave processes on coral reef flats: implications for reef geomorphology using Australian case studies, 1072. Journal of Coastal Research 22, 209–223 http://dx.doi.org/10.2112/05A-0016.1.
Klonowski, W., Gray, M., Majewski, L., Lynch, M., Fearns, P., 2010. Ningaloo collaboration cluster: hyperspectral mapping of Bathymetry and Benthic Cover. Ningaloo Collaboration Cluster Final Report, 18 June 2010.
Lee, T.T., Black, K.P., 1978. The energy spectra of surf waves on a coral reef. Proc.16th Int. Conf. Coastal Eng., ASCE, pp. 588–608.
Lindemer, C.A., Plant, N.G., Puleo, J.A., Thompson, D.M., Wamsley, T.V., 2010. Numerical simulation of a low-lying barrier island's morphological response to Hurricane Katrina. Coastal Engineering (ISSN: 0378-3839) 57 (11-12), 985–995 http://dx.doi.org/10.1016/j.coastaleng.2010.06.004 (November-December 2010).
Longuet-Higgins, M.S., Stewart, R.W., 1964. Radiation stress in water waves: a physical discussion with applications. Deep Sea Research 11, 529–562.
Lowe, R.J., Falter, J.L., Bandet, M.D., Pawlak, G., Atkinson, M.J., Monismith, S.G., Koseff, J.R., 2005. Spectral wave dissipation over a barrier reef. Journal of Geophysical Research 110, C04001 http://dx.doi.org/10.1029/2004JC002711.
Lowe, R.J., Falter, J.L., Koseff, J.R., Monismith, S.G., Atkinson, M.J., 2007. Spectral wave flow attenuation within submerged canopies: Implications for wave energy dissipation. Journal of Geophysical Research 112, C05018 http://dx.doi.org/10.1029/2006JC003605.
Lowe, R.J., Shavit, U., Falter, J.L., Koseff, J.R., Monismith, S.G., 2008. Modeling flow in coral communities with and without waves: a synthesis of porous media and canopy flow approaches. Limnology and Oceanography 53 (6), 2668–2680.
Lowe, R.J., Falter, J.L., Monismith, S.G., Atkinson, M.J., 2009a. Wave-driven circulation of a coastal reef-lagoon system. Journal of Physical Oceanography 39 (4), 873–893.
Lowe, R.J., Falter, J.L., Monismith, S.G., Atkinson, M.J., 2009b. A numerical study of circulation in a coastal reef lagoon system. Journal of Geophysical Research 114, C06022 http://dx.doi.org/10.1029/2008JC005081.
Lugo-Fernandez, A., Roberts, H.H., Wiseman, W.J., Carter, B.L., 1998. Water level and currents of tidal and infragravity periods at Tague Reef, St. Croix (USVI). Coral Reefs 17 (4), 343–349.
Massel, S.R., Gourlay, M.R., 2000. On the modelling of wave breaking and set-up on coral reefs. Coastal Engineering 39, 1–27.
McCall, R.T., Van Thiel de Vries, J.S.M., Plant, N.G., Van Dongeren, A.R., Roelvink, J.A., Thompson, D.M., Reniers, A.J.H.M., 2010. Two-dimensional time dependent hurricane overwash and erosion modelling at Santa Rosa Island. Coastal Engineering 57 (7), 668–683 http://dx.doi.org/10.1016/j.coastaleng.2010.02.006.
Munk, W.H., Sargent, M.C., 1948. Adjustment of Bikini Atoll to ocean waves. Transactions of the American Geophysical Union 29, 855–860.
Nwogu, O., Demirbilek, Z., 2010. Infragravity wave motions and runup over shallow fringing reefs. ASCE Journal of Waterway, Port, Coastal, and Ocean Engineering http://dx.doi.org/10.1061/(ASCE)WW.1943-5460.0000050.
Ogg, J.G., Koslow, J.A., 1978. The impact of typhoon Pamela, 1976, on Guam's coral reefs and beaches. Pacific Science 32, 105–118.
Okihiro, M., Guza, R.T., 1995. Infragravity energy modulation by tides. Journal of Geophysical Research 100, 16,143–16,148.
Péquignet, A.C.N., Becker, J.M., Merrifield, M.A., Aucan, J., 2009. Forcing of resonant modes on a fringing reef during tropical storm Man-Yi. Geophysical Research Letters 36, L03607 http://dx.doi.org/10.1029/2008GL036259.
Phillips, O.M., 1977. The Dynamics of the Upper Ocean, 336 pp. Cambridge University Press, New York.
Pomeroy, A., Lowe, R., Symonds, G., Van Dongeren, A., Moore, C., 2012. The dynamics of infragravity wave transformation over a fringing reef. J. Geophys. Res. 117, C11022, http://dx.doi.org/10.1029/2012JC008310.
Ranasinghe, R., Turner, I.L., Symonds, G., 2006. Shoreline response to multi-functional artificial surfing reefs: a numerical and physical modelling study (2006). Coastal Engineering 53 (7), 589–611.
Reniers, A.J.H.M., Van Dongeren, A.R., Battjes, J.A., Thornton, E.B., 2002. Linear modelling of infragravity wave response during Delilah. Journal of Geophysical Research 107 (C10), 3137 http://dx.doi.org/10.1029/2001JC001083.
Reniers, A.J.H.M., Roelvink, J.A., Thornton, E.B., 2004. Morphodynamic modeling of an embayed beach under wave group forcing. Journal of Geophysical Research, C: Oceans 109 (1), C01030 http://dx.doi.org/10.1029/2002JC001586 (1-22).
Roeber, V., Cheung, K.F., 2012. Boussinesq-type model for energetic breaking waves in fringing reef environments. Coastal Engineering (ISSN: 0378-3839) 70, 1–20 http://dx.doi.org/10.1016/j.coastaleng.2012.06.001 (December 2012).
Roelvink, J.A., 1993. Dissipation in random wave groups incident on a beach. Coastal Engineering 19, 127–150.
Roelvink, J.A., Reniers, A., Van Dongeren, A., Van Thiel de Vries, J., McCall, R., Lescinski, J., 2009. Modeling storm impacts on beaches, dunes and barrier islands. Coastal Engineering http://dx.doi.org/10.1016/j.coastaleng.2009.08.006.
Rosman, J.H., Hench, J.L., 2011. A framework for understanding drag parameterizations for coral reefs. Journal of Geophysical Research 116, C08025 http://dx.doi.org/10.1029/2010JC006892.
Ruessink, B.G., Kleinhans, M.G., van den Beukel, P.G.L., 1998. Observations of swash under highly dissipative conditions. Journal of Geophysical Research 103, 3111–3118.
Ruessink, B.G., Miles, J.R., Feddersen, F., Guza, R.T., Elgar, S., 2001. Modeling the alongshore current on barred beaches. Journal of Geophysical Research 106, 22451–22463.
Schaeffer, H.A., 1993. Infragravity wave induced by short-wave groups. Journal of Fluid Mechanics 247, 551–588.
Senechal, N., Bonneton, P., Dupuis, H., 2001. Field observations of irregular wave transformation in the surf zone. Coastal Dynamics '01. Am. Soc. of Civ. Eng., Reston, Va, pp. 62–71.
Sheremet, A., Kaihatu, J.M., Su, S.-F., Smith, E.R., Smith, J.M., 2011. Modeling of nonlinear wave propagation over fringing reefs. Coastal Engineering (ISSN: 0378-3839) 58 (12), 1125–1137 http://dx.doi.org/10.1016/j.coastaleng.2011.06.007 (December 2011).
Storlazzi, C.D., Ogston, A.S., et al., 2004. Wave- and tidally-driven flow and sediment flux across a fringing coral reef: Southern Molokai, Hawaii. Continental Shelf Research 24 (12), 1397–1419.
Storlazzi, C.D., Elias, E., Field, M.E., Presto, M.K., 2011. Numerical modeling of the impact of sea-level rise on fringing coral reef hydrodynamics and sediment transport. Coral Reefs 30 (1), 83–96 http://dx.doi.org/10.1007/s00338-011-0723-9.
Svendsen, I.A., 1984. Mass flux and undertow in the surf zone. Coastal Engineering 8, 347–365.
Symonds, G., Black, K.P., 2001. Predicting wave-driven currents on surfing reefs. Journal of Coastal Research Special Surfing Issue 29, 102–114.
Symonds, G., Huntley, D.A., Bowen, A.J., 1982. Two dimensional surf-beat: long wave generation by a time-varying break point. Journal of Geophysical Research 87 (C1), 492–498.
Symonds, G., Black, K.P., Young, I.R., 1995. Wave-driven flow over shallow reefs. Journal of Geophysical Research 100, 2,639–2,648.
Taebi, S., Lowe, R.J., Pattiaratchi, C.B., Ivey, G.N., Symonds, G., Brinkman, R., 2011. Nearshore circulation in a tropical fringing reef system. Journal of Geophysical Research, Oceans 116, C02016 http://dx.doi.org/10.1029/2010JC006439.
Thomson, J., Elgar, S., Raubenheimer, B., Herbers, T.H.C., Guza, R.T., 2006. Tidal modulation of infragravity waves via nonlinear energy losses in the surfzone. Geophysical Research Letters 33 (5).
Van Dongeren, A.R., Reniers, A.J.H.M., Battjes, J.A., Svendsen, I.A., 2003. Numerical modeling of infragravity wave response during Delilah. Journal of Geophysical Research 108 (C9), 3288 http://dx.doi.org/10.1029/2002JC001332.
Wolanski, E., Sarsenski, J., 1997. Larvae dispersion in coral reefs and mangroves. American Scientist 85 (3), 236–243.
Zhang, Z., Lowe, R.J., Falter, J., Ivey, G., 2011. A numerical model of wave- and current-driven nutrient uptake by coral reef communities. Ecological Modelling 222, 1456–1470.